Analysis of an infrared mirage sequence

Waldemar H. Lehn

Infrared observations of seaborne thermal sources are subject to the effects of atmospheric refraction. For low elevation angles at long ranges, out to the limit of visibility, the inevitable atmospheric temperature gradients frequently produce mirages. I present an analysis of a 22-min sequence of images recorded on 18 February 1994 at the U.S. Naval Surface Warfare Center at Wallops Island, Virginia. The infrared target is a heat source carried on a ship moving in a straight line toward the camera. The images show a quasi-periodic variation of the horizon elevation, as well as an extended range of visibility. A model that reasonably reproduces the observed features consists of a small temperature inversion in a slightly sloped atmosphere, with an atmospheric gravity wave moving across the line of sight.

Key words: Infrared mirage, atmospheric refraction.

1. Introduction

All long-range optical observations are affected by refraction in the atmosphere. A well-known example is astronomical refraction that creates a small apparent vertical displacement of a star or distant object. Refraction within the surface layer, however, is not always uniform and on occasion can cause considerable distortion. If an observation is sufficiently disrupted, it is recognized as a mirage. Phenomena that can occur include shortening or lengthening of the nominal horizon distance, seeing far beyond the normal horizon, and seeing multiple elevated images of a single source.

In a set of experiments carried out at the U.S. Naval Surface Warfare Center, Dahlgren Division, in the Horizon Infrared Surveillance Sensor program, infrared images of distant thermal targets have frequently been affected by mirages. A detailed description of the research program is given by Trahan[1] and Bauer.[2] The points relevant to this paper are summarized below.

The field tests were carried out at an experimental site located on Wallops Island, Virginia. Two types of sensor were mounted, with the objective of long-range over-water observation and detection of infrared sources. Experimentally, two principal lines of sight through the marine surface layer were used: (i) parallel to shore at a nominal bearing angle of 199° toward a fixed station, where the target was a heat source that could be moved up or down a mast (elevations 4.4–26.6 m above mean sea level) and (ii) directly out to sea at nominal bearing 130°, observing a heat source target on a ship sailing directly toward or away from the test site, with two possible target elevations aboard the ship [12 ft (3.7 m) or 21 ft (6.4 m) above sea level].

The images of interest here were received by the infrared propagation camera situated at an elevation of 22.0 m above mean sea level. The camera's sensor array, of dimension 256×256 pixels, was sensitive to infrared radiation in the wavelength range 3.9–5.1 μm. The lens had a very long focal length, such that the whole field of view was $0.48° \times 0.48°$. For comparison purposes, the equivalent lens for a 35-mm camera would have a focal length of approximately 3 m.

Although it is easily recognized that mirages cause these observations, detailed models that reproduce the observations are not available. My objective is to present such a model for one specific observation sequence and to explain the general features, trends, and causes of the observations, without necessarily reproducing all the finer details.

2. Observed Sequence

The sequence that is examined here was videotaped on 18 February 1994 during an inbound run of the ship *Sea Lion* along the line bearing 130°. The ship's speed, based on positional information provided by Trahan,[3] was 19.8 knots (10.2 m s^{-1}), and the ship's distance d from the camera, with t ex-

The author is with the Department of Electrical and Computer Engineering, University of Manitoba, Winnipeg R3T 5V6, Canada.

Received 18 June 1996.
0003-6935/97/215217-07$10.00/0

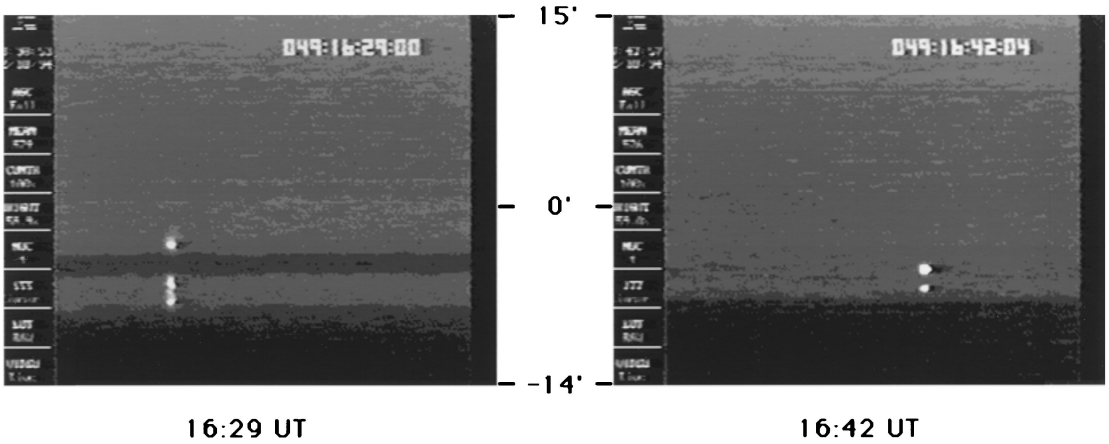

Fig. 1. Typical full-frame images captured from the video recording. The vertical scale gives angular elevation in arc minutes. In the data imprinted in the upper right-hand corner, the first three digits give the day of the year in 1994, whereas the remaining digits define the time of the exposure in UT. At 16:29 the ship's distance is 35.0 km; at 16:42 it is 27.0 km.

pressed in the form of hours:minutes, was $d = 0.611(16{:}43 - t) + 26.4$ km. The infrared source on the ship was mounted at the 21-ft elevation (6.4 m above sea level).

Under a standard atmosphere with a surface temperature of 10 °C and a lapse rate of 0.006 °C m^{-1}, the horizon elevation is −2.40 mrad (−8.25 arc min) and the horizon distance is 18.5 km. The heat source at elevation 6.4 m would be visible to a distance of 28.5 km, beyond which it would disappear beneath the horizon. The orientation of the infrared propagation camera was fixed so that the nominal horizon would appear approximately one fifth of the way up from the bottom of the image frame, although the exact elevation angle of the optical axis was not measured. This information, when combined with the frame height of 0.48°, produces a standard image of height 29 arc min, with the bottom edge of the frame having an elevation angle of −14 arc min.

Figure 1 shows two typical frames from the recording. The date and Universal Time (UT) are imprinted on the images. Some indication of the prevailing atmospheric conditions is given by the air–sea temperature difference, where the air temperature is measured at least 2 m above the sea; its value was +1.3 °C during the observations.

The video, spanning the time interval from 16:22 to 16:43 UT, shows interesting and complex mirages. The horizon moves up and down; the image of the sea sometimes splits into two, with sky showing in between; and the image of the heat source appears, disappears, and changes from single to multiple images stacked one above the other. For this study, frames were captured from the video at every whole minute, with 22 frames in all. This choice of a 60-s sampling interval was based on the rate at which the video images evolved; the heater's image flickered and jittered with a time scale of a few seconds, but the major features changed more slowly. The images of the heat source were extracted and assembled side by side to create Fig. 2, in which the direction of increasing time is toward the left, whereas the ship's distance increases toward the right.

In Fig. 3, which is an outline sketch of Fig. 2, it can

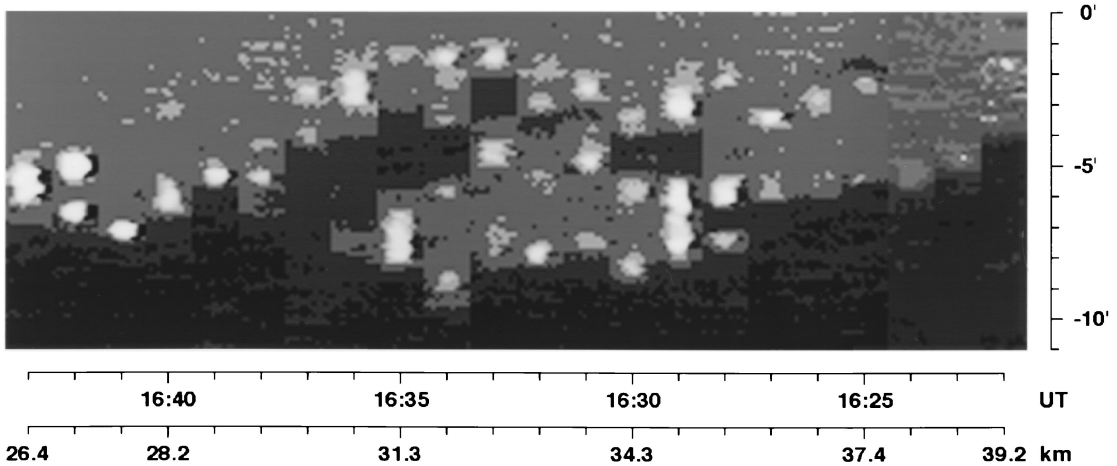

Fig. 2. Composite image of the observations. The vertical scale gives elevation in arc minutes. The upper horizontal scale gives the time of each observation in the form of hours:minutes UT; the lower scale gives the ship's distance at that moment.

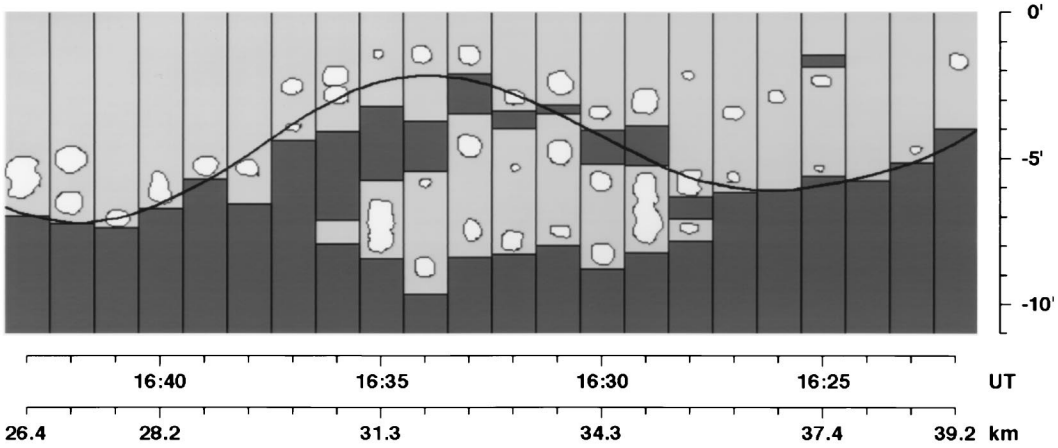

Fig. 3. Schematic outline of Fig. 2, using the same scales. The significant features of the images are emphasized: the dark gray regions are images of the cold sea surface, light gray represents the sky, and white is the image of the heat source. A wavelike curve has been added by hand to point out the quasi-sinusoidal variation of the upper horizon level.

be seen that the elevation of the upper horizon varies in quasi-sinusoidal fashion, with a period of approximately 16 min. In other words, the horizon configuration more or less repeats itself in this time. The sketched-in wave has its minima at 16:26 and 16:42 (ship's distances are, respectively, 36.8 and 27.0 km) and its maximum at 16:34 (ship at 31.9 km). This observation suggests the existence of a wave phenomenon in the atmosphere.

3. Mirages

The physics of mirage formation is well understood, although not easily accessible in the form of a modern English language reference text. The classic standard reference book, written by Pernter and Exner,[4] dates from 1922; the books by Fleagle and Businger[5] and by Greenler[6] also contain relevant discussions. The mathematics of ray tracing was further extended by Fraser[7] and Tape,[8] and a simplified model that computes rapidly was developed by Lehn.[9]

To review the main points of mirage formation briefly: Light rays pass through the atmosphere on slightly curved paths, with the curvature κ being a function of the refractive-index gradient[10]

$$\kappa = \frac{1}{n}\,\hat{\nu}\cdot\nabla n,$$

where n is the refractive index of air and $\hat{\nu}$ is the unit vector normal to the ray and pointing toward the center of curvature.

The refractive index exhibits a slight dependence on wavelength, but for the near-infrared range in question it is little different from the visible light values. The Cauchy formula[11] for air, valid from the visible to at least 9 μm, states that, at standard temperature and pressure, $n - 1 = A_1(1 + B_1/\lambda^2)$, where $A_1 = 28.79 \times 10^{-5}$ and $B_1 = 5.67 \times 10^{-11}$ when wavelength λ is expressed in centimeters. Thus, for visible light of wavelength 0.55 μm, $n - 1 = 2.93 \times 10^{-4}$, whereas for infrared radiation at 4 μm, the value is 2.88×10^{-4}. This small difference of less than 2% will be neglected in the following discussion, and the visible light formulas will be applied.

Air temperature, the parameter that most profoundly affects refraction, is related to refractive index through the density of air ρ: $n = 1 + \varepsilon\rho = 1 + \varepsilon\beta p/T$, where p is atmospheric pressure, T is temperature in degrees Kelvin, and ε and β are constants: $\varepsilon = 226 \times 10^{-6}$ and $\beta = 3.48 \times 10^{-3}$ in SI units. In a spherically symmetric atmosphere concentric with the Earth, in which the static gravitational pressure equation $\mathrm{d}p/\mathrm{d}z = -g\rho$ holds, the relation for curvature then becomes

$$\kappa = \frac{\varepsilon\beta}{nT}\left(g\beta + \frac{\mathrm{d}T}{\mathrm{d}z}\right)\cos\phi,$$

where z is elevation above the Earth's surface and ϕ is the elevation angle of the ray's tangent. This equation gives a positive result if a ray is concave downward. Since curvature is in all cases a small number, the circular arcs it defines can be replaced by parabolic arcs to greatly simplify computation.

An atmosphere of the type just described will in the ensuing sections be termed flat. Such an atmosphere is indeed locally flat, i.e., it is described approximately by a set of parallel planes tangent to the Earth. This terminology is introduced to distinguish it from atmospheres in which the isothermal surfaces are not spherical. Note that, in the results presented here, the calculations always account for the curvature of the Earth.

Two modifications are made to the flat atmosphere. The first of these, whose necessity is discussed below, permits the parallel layers to possess a very small slope, of the order of a few arc minutes, relative to the Earth. The second is the addition of gravity waves that produce sinusoidal undulations in isothermal surfaces.

Gravity waves can exist in stably stratified atmospheres such as those present under a temperature inversion.[12] The model used in this application has been exactly described elsewhere,[13] and details are

not repeated here. It consists of a four-layer inversion with no wind. In each layer the temperature varies linearly with elevation. Solving the wave equations yields the dispersion relation, which gives the wave numbers that can exist for a given frequency. For the observed fundamental period of 16 min, a discrete set of wave numbers is possible. This set of values depends strongly on the shape of the temperature profile selected.

The waves convert each isothermal surface (originally flat) into the shape of a sinusoidal plane wave propagating along the line of sight. The amplitude of a wave depends on the elevation at which it is travelling: zero amplitude at ground level and generally a maximum in the zone of most rapid temperature increase within the inversion.

The discrete wave numbers, which assume that the waves travel along the line of sight, are not as restrictive as might first be supposed. If the wave vector makes an angle with the line of sight, the effective wave number seen by the observer becomes smaller, although the frequency remains the same; the observer simply sees the effect of a longer wavelength. When the angle approaches 90°, for a wave transverse to the line of sight, the effective wavelength becomes infinite and the model can be simplified with little loss of accuracy to a vertical oscillation of the layers in the flat atmosphere.

A stable atmosphere can simultaneously support many different frequencies and their corresponding wave numbers (modes), but in this analysis only one or two modes will be used.

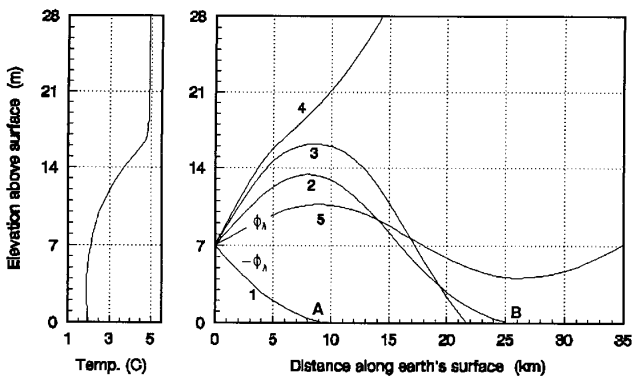

Fig. 4. Properties of a duct in a flat atmosphere. Several rays are shown entering the observer's eye at an elevation of 7 m, at 0 km on the distance scale. For purposes of discussion and computation, the rays are considered to propagate in the reverse direction, so that the ray bundle emanates from the observer's eye. Ray 1 at elevation angle $-\phi_h$, tangent to the surface of the sea at A, defines the lower horizon. Ray 2 at angle ϕ_h, returned by the refraction at the inversion, is symmetrical about its vertex; when it returns to the level of the observer its angle is $-\phi_h$, and it is necessarily tangent to the sea also (at B). This defines the lower edge of an elevated and inverted sea image. Ray 3 is returned by even stronger refraction, and because its angle upon return to the observer's level is steeper than $-\phi_h$, it must strike the sea; the observer sees an image of the sea higher than ϕ_h. Ray 4 is sufficiently steep to penetrate the inversion, passing upward and generating a sky image. Ray 5 is the ducted ray. Its angle is too shallow to intersect the sea and also too shallow to penetrate the inversion. It is thus trapped in a duct bounded by the inversion and the sea, within which it proceeds in cyclical fashion.

4. Reconstruction

Given the knowledge of target shape, mirage appearance, and range, one would like to be able to calculate directly the temperature profile of the intervening atmosphere. Several such direct inversion techniques have been developed,[14–16] but they all incorporate limiting assumptions that make them unsuitable for the case of optical ducting. It is also possible to begin with a thermodynamic model,[17] with which temperature profiles are calculated from known wind shear and air–sea temperature differences. This model has its limits as well; at very low wind speeds the atmospheric stability becomes extreme and unpredictable temperature inversions develop.

This study is therefore based on a search through different postulated temperature profiles, guided by field experience in mirage observation, and many previous simulations. The atmospheres were kept as simple as possible, with minimal temperature excursions.

The easiest way to model the 16-min periodic variation of the upper horizon is a gravity wave that propagates at right angles to the line of sight. For compactness this is called a transverse wave. At any instant a bundle of rays passing from target to observer does not encounter the wavy nature of the atmosphere, since the rays are parallel to the wavefronts. As time proceeds, the atmosphere simply appears to move up or down.

Other possible configurations were also investigated, especially gravity waves moving along the line of sight. But for typical inversions, the wave numbers associated with the 16-min period were too large. The corresponding wavelengths, of the order of 1–5 km, were not able to reproduce the large observed horizon variation.

From the outset it was assumed that the model must, for some parameter values, permit an optical duct to exist. Ducting is evident in the images for

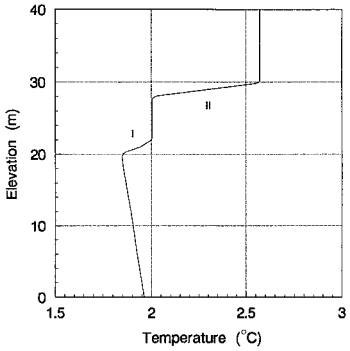

Fig. 5. Temperature profile that approximately reproduces the horizon variation. The camera elevation is 22 m, and the profile is shown in its highest position.

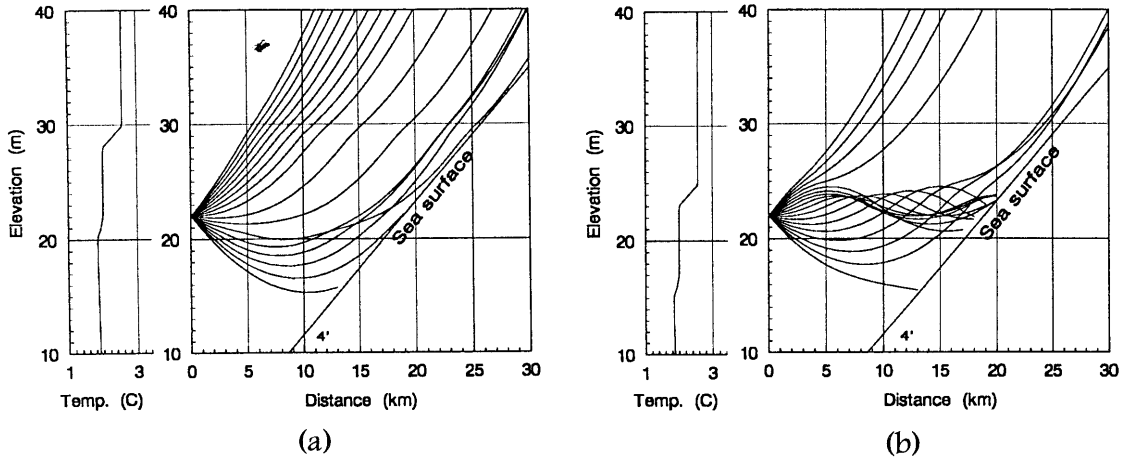

Fig. 6. Ray traces for the extreme positions of the temperature profile. The effect of the inversion in refracting rays downward can be seen. The isothermal layers of the atmosphere, considered to have a downward slope of 4 arc min, are shown here as level; to compensate, the sea surface is drawn as a line sloping upward by 4 arc min. Ray elevation angles at the camera span the range (−4 to +4 arc min), at 0.5-arc min intervals; when the layer slope is added, the true elevation range becomes (−8 to 0 arc min). (a) The inversion has its highest position above the camera. Rays enter the region of strong gradient so steeply that they penetrate it, and pass up into the sky. (b) When the inversion has its lowest position, rays have a shallower angle as they enter the strong gradient. These rays are refracted downward, trapped beneath the inversion.

16:28 to 16:36: A window appears between two dark regions. The lower dark region is clearly the expected one of the cold dark sea, whereas the upper one is an elevated mirage of the sea. Within the window one sees the lighter sky, as well as long range images of the heat source on the ship. This part is the manifestation of the duct that traps light rays and transmits them around the curve of the earth.[18] A duct places constraints on the ray paths and hence on the temperature profile. Consider the necessary ray paths from the observer's point of view (Fig. 4). Rays entering the eye at low elevation angles produce the expected image of the sea. The middle rays, next above these, come from the sky, but the next higher rays come from the sea again. These last rays, emanating upward from the sea, are returned to the eye by strong refraction at the inversion. The middle rays on the other hand do not intersect the sea; they propagate fairly normally below the inversion and are only mildly refracted at the inversion; they remain trapped below the inversion, and make up the ducted image. The corresponding temperature profile typically has a small gradient from the sea upward, capped by a fairly sharp temperature increase containing gradients well above 0.1 K m^{-1}.

If a duct exists in a flat atmosphere it automatically possesses certain symmetries. Thus an unobstructed ducting ray crossing the level of the observer's eye at an angle $+\phi$ will at some other point cross this level at angle $-\phi$. If the lower sea horizon is at angle $-\phi_h$, then an upward ray $+\phi_h$ returned by the inversion will also intersect the sea. The duct then spans the range $(-\phi_h, +\phi_h)$, symmetric about zero elevation.

Now the center of the observed duct varies in elevation from approximately −6 to −7 arc min. This loss of symmetry can be remedied in the model by imposing a small slope on the flat atmosphere, letting its parallel planes slope downward at an angle θ relative to the horizontal.[19] In terms of the concentric spherical atmospheric shells, their normals would now make an angle θ with the normal to the earth's surface.

The observed images vary between two extremes: a wide duct with the upper horizon at −2 arc min, and no duct with the horizon at −7 arc min. Synthesis was attempted of an atmosphere that would reproduce the variation in appearance of the horizon and duct, ignoring for the moment the position of the ship itself.

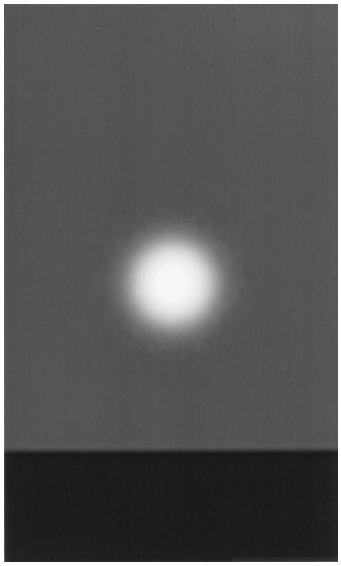

Fig. 7. Source image for the mirage simulation. The heat source is located 6.4 m above sea level. At the distances in question, the heater would look like a point source. However the fuzzy image used here produces simulations more like the observations, all of which show distinctly diffused images that result from slight irregularities in the long optical path.

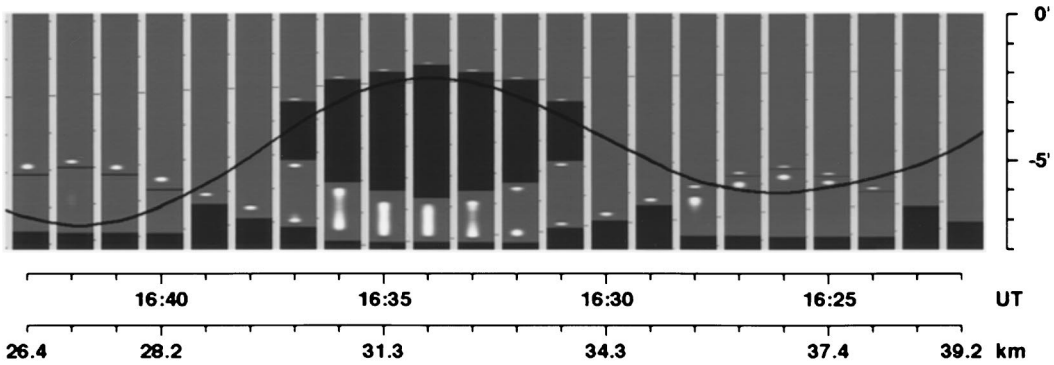

Fig. 8. Calculated image sequence in the presence of the transverse wave only. For comparison the wave from Fig. 3 has been superimposed.

After numerous trials that were an attempt to account for the constraints on ray direction for the different parts of the ray bundle, the profile of Fig. 5 was chosen. With the inversion at its highest level, as in the figure, the appearances of the 16:26 and 16:42 images are obtained, whereas at its lowest level, a moderate approximation to the 16:34 image occurs. Figure 6 shows the ray traces for these cases. Atmospheric slopes of from -6 to -7 arc min, values suggested by the asymmetric center position of the ducts, were found to produce less satisfactory results than the value of -4 arc min that was ultimately chosen for the slope. Each of the two positive gradients in the temperature profile (Fig. 5) has a definite function. When the atmosphere is at its highest level, the observer's eye is near region I; steep downward rays are not much affected, and the observed horizon of -8 arc min is seen. At the same time, upward rays meet region II sufficiently steeply that they pass through it (no duct). As the profile is lowered, however, downward rays are somewhat straightened by region I (raising the horizon, as observed), whereas upward rays, entering region II less steeply, begin to be refracted downward (making the duct).

If the atmosphere is now moved up and down between these extremes, in sinusoidal fashion with 16-min periods, an approximation of the observed horizon variation is achieved. The equation for the vertical atmospheric displacement is

$$y = 2.5 \cos\left[\frac{2\pi}{16}(t - 16{:}26)\right] - 2.5 \text{ m},$$

where y is the displacement of the temperature curve relative to the position shown in Fig. 5. In Section 5 the images of the ship's heat source are added and the simulation results presented.

It should be mentioned here that this vertical oscillation of the air is not an exact model for the gravity waves. The sea surface imposes a boundary condition of zero vertical displacement and velocity on atmospheric movement. As a result, the isothermal surfaces in the inversion are alternately compressed and rarified as the wave passes. When the variation of layer thicknesses at the critical refracting levels (steepest temperature gradients) were checked, however, they were found to be minimal. This justified use of the simpler model with its attendant higher computational speed.

It should also be noted that it is the shape of the temperature profile, rather than the absolute temperature, that determines the nature of the mirage; the whole profile can be shifted up or down by a few degrees without noticeably affecting the mirage.

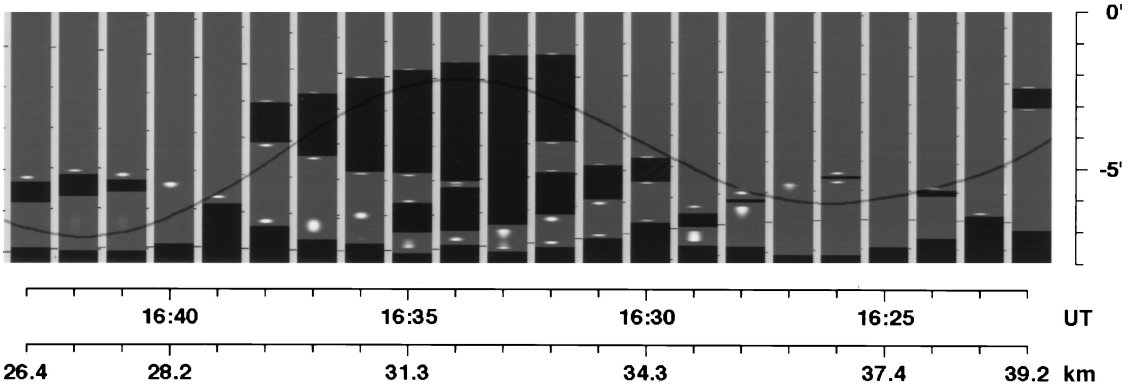

Fig. 9. Image sequence that includes fine structure that is due to a second, small amplitude wave mode.

5. Results

Rays were traced for each ship's position corresponding to the full minute, and a mirage was simulated for that case. The mirage simulation[20] used the simple representation shown in Fig. 7 for the heat source on the ship. The figure shows nothing of the ship itself, because the observed images likewise recorded no such details. The calculated mirages are then assembled in Fig. 8 for comparison with the observation.

The general trend of the result shows clear similarities with the observation without being identical. For comparison, the wave sketched over the observation in Fig. 3 is superimposed. The horizon variation and the ducts are reasonably similar. Recall that this result is for the transverse wave alone.

Now the observation shows a wealth of fine structure, for which there are several possible sources. One is a swell in the ocean, which would generally exist even though the air during the observation was calm. A swell could easily change the ship's vertical position by ± 0.5 m; this has been verified to produce significant changes in the appearance of the heat source, e.g., from single to multiple images or vice versa. The other possibility is a second gravity wave superimposed on the first. A few tests, with wavelengths of the order of 2.5, 5, and 10 km, showed that even a small amplitude wave of this sort would introduce a lot of fine structure. A sample of this is shown in Fig. 9, where a secondary wave was added to show the general trend of possible effects; additional time and effort were not expended to get a more exact fit. Here a secondary wave traveling away from the observer is superimposed, with wavelength 10.5 km, period 13.3 min, and amplitude 0.35 m at the upper inversion level. The period corresponds to an angular frequency of 0.0079 rad/s, for which the lowest wave number possible in this atmosphere is 0.01 m^{-1}. For the observer to see a wavelength of 10.5 km (wave number 0.0006 m^{-1}), the wave must travel almost perpendicularly to the line of sight, with the wave vector making an angle of 86° with it.

There can be no assurance that this is a unique representation of the observation, but of the many variations investigated, this was the only one that was even adequate in reproducing the trends of the observed sequence. The constraints on the model were many, requiring a prescribed temporal variation of the sea image, and then a specified track of the target heat source as it approached from 39 to 26 km. Models that fit the sea image usually failed when the moving target was added. There is also an interesting similarity to the stepped inversion studied by Church[17]; he used the same image data but his objective was to show the possible range of image variation with flat atmospheres without attempting to model all the temporal variation.

6. Conclusions

Mirages in the near infrared have basically the same characteristics as those in visible light. To reproduce the observed infrared mirage sequence, a gravity wave model is required, consisting of a set of waves moving along a small temperature inversion in a slightly sloping atmosphere. The basic quasi-sinusoidal elevation variation of the upper horizon is produced by a wave of 2.5-m amplitude moving across the line of sight at right angles. The fine structure involving the varying appearances of the ship's heat source can be attributed to one or more further waves of smaller amplitude superimposed on the first.

The author thanks E. Bauer and J. W. Trahan for numerical data and helpful discussions, the U.S. Naval Surface Warfare Center, Dahlgren Division, for providing a video recording of the observation, and Scott Polar Research Institute, University of Cambridge, for providing visiting scholar facilities.

References and Notes

1. J. W. Trahan, "Infrared refraction and mirages," in *Proceedings 1995 Infrared Information Symposium* (*IRIS*), *Specialty Group on Targets, Background and Discrimination* (*TBD*), Vol. 1 (1995) pp. 185–210.
2. E. Bauer, "Effects of atmospheric refraction on long-range near-surface electro-optical sensing over water," document D-1816 (Institute for Defense Analyses, Alexandria, Va., 1996).
3. J. W. Trahan, Naval Surface Warfare Center, Dahlgren, Va. (personal communication, 6 November 1995).
4. J. M. Pernter and F. Exner, *Meteorologische Optik*, 2nd ed. (Braumüller, Vienna, 1922).
5. R. G. Fleagle and J. A. Businger, *An Introduction to Atmospheric Physics*, 2nd ed. (Academic, New York, 1980).
6. R. Greenler, *Rainbows, Halos, and Glories* (Cambridge U. Press, Cambridge, U.K., 1980).
7. A. B. Fraser, "Solutions of the refraction and extinction integrals for use in inversions and image formation," Appl. Opt. **16,** 160–165 (1977).
8. W. Tape, "The topology of mirages," Sci. Am. **252,** 100–129 (1985).
9. W. H. Lehn, "A simple parabolic model for the optics of the atmospheric surface layer," Appl. Math. Model. **9,** 447–453 (1985).
10. M. Born and E. Wolf, *Principles of Optics*, 6th ed. (Pergamon, Oxford, 1986), Sect. 3.2.1.
11. Ref. 10, Sect. 2.3.4.
12. E. E. Gossard and W. H. Hooke, *Waves in the Atmosphere* (Elsevier, New York, 1975).
13. W. H. Lehn, W. K. Silvester, and D. M. Fraser, "Mirages with atmospheric gravity waves," Appl. Opt. **33,** 4639–4643 (1994).
14. W. H. Mach and A. B. Fraser, "Inversion of optical data to obtain a micrometeorological temperature profile," Appl. Opt. **18,** 1715–1723 (1979).
15. W. H. Lehn, "Inversion of superior mirage data to compute temperature profiles," J. Opt. Soc. Am. **73,** 1622–1625 (1983).
16. W. G. Rees, C. M. Roach, and C. H. Glover, "Inversion of atmospheric refraction data," J. Opt. Soc. Am. A **8,** 330–338 (1991).
17. S. R. Church, "Atmospheric mirage and distortion modeling for IR target injection simulations," in *Meeting on Targets and Backgrounds: Characterization and Representation II*, W. R. Watkins, ed., Proc. SPIE **2742,** 122–135 (1996).
18. W. H. Lehn, "The Novaya Zemlya effect: an arctic mirage," J. Opt. Soc. Am. **69,** 776–781 (1979).
19. Slopes have been introduced in a previous simulation [W. H. Lehn and B. German, "Novaya Zemlya effect: analysis of an observation," Appl. Opt. **20,** 2043–2047 (1981)]. Such a slope is also recognized as necessary in Ref. 17, in which advection is considered capable of producing the small values in question.
20. W. H. Lehn and W. Friesen, "Simulation of mirages," Appl. Opt. **31,** 1267–1273 (1992).